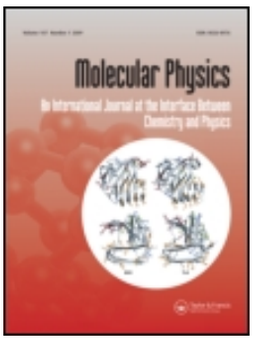

Molecular Physics

ISSN: 0026-8976 (Print) 1362-3028 (Online) Journal homepage: http://www.tandfonline.com/loi/tmph20

Molecular-dynamics studies and neutron-scattering experiments on methylene chloride

Gerald R. Kneller & Alfons Geiger

To cite this article: Gerald R. Kneller & Alfons Geiger (1990) Molecular-dynamics studies and neutron-scattering experiments on methylene chloride, Molecular Physics, 70:3, 465-483, DOI: 10.1080/00268979000101131

To link to this article: http://dx.doi.org/10.1080/00268979000101131

MOLECULAR PHYSICS, 1990, VOL. 70, NO. 3, 465–483

Molecular-dynamics studies and neutron-scattering experiments on methylene chloride

Part II: Dynamics

by GERALD R. KNELLER†
Institut für Physikalische Chemie der RWTH Aachen, Templergraben 59, D-5100 Aachen, West Germany

and ALFONS GEIGER
Physikalische Chemie, Fachbereich Chemie der Universität Dortmund, Otto-Hahn-Strasse, D-4600 Dortmund, West Germany

(*Received 28 September 1989; accepted 21 December 1989*)

We calculate inelastic neutron-scattering intensities of methylene chloride for cold neutrons from molecular-dynamics (MD) simulations and compare them with experimental data. To obtain realistic scattering intensities, the effect of multiple scattering is taken into account by a Monte Carlo (MC) simulation, using the dynamic structure factor calculated from our MD simulations as input. The MD simulations of methylene chloride are performed with the same potentials as in Part I of this work. The dynamic structure factor is calculated using fast correlation algorithm (FCA), which is based on the fast-Fourier-transform (FFT) algorithm and the Wiener–Khinchin theorem for discrete functions.

1. Introduction

Neutron-scattering experiments cover the whole range in space *and* time accessible by molecular dynamics (MD) simulations and therefore provide unique experimental data to test the validity of such simulations. Usually 'idealized' scattering intensities are calculated from the simulations and compared with experimental results. The experimental intensities are corrected for effects not involving the internal structure and dynamics of the sample, such as background scattering or detector efficiency, as well as for effects like multiple scattering, and (in the case of diffraction experiments) inelastic scattering that do require knowledge of space and time correlations of the sample.

It is tempting to include these 'non-trivial' effects in the simulation process. Unfortunately, this method is limited since the dynamic structure factor, the basic quantity of interest, is calculated from MD trajectories by classical time averages, and, to account for detailed balance and recoil, a semiclassical correction with a limited validity concerning the momentum transfer q and energy transfer $\hbar\omega$ has to be applied.

In Part I of this work [1] we gave the bounds for the (q, ω) region that can be covered by MD simulations of molecular liquids:

$$|\hbar\omega| < k_B T, \tag{1}$$

† Present address: IBM Corporation, Department 48B/MS 428, Neighbourhood Road, Kingston, New York 12401, U.S.A.

0026-8976/90 $3.00

$$\frac{\hbar^2 q^2}{2M} \ll 2k_B T. \tag{2}$$

M is the lowest effective mass of the atoms forming one molecule. We pointed out that, owing to these bounds, simulations of realistic neutron-*diffraction* experiments cannot be carried out for molecular liquids such as methylene chloride whose molecules contain hydrogen atoms with low effective masses. For such liquids simulations of inelastic neutron-scattering spectra in the *low-q region*, where the conditions (1) and (2) are fulfilled, provide an additional useful test of MD potentials.

The procedure is then as follows. In the first step one has to calculate the dynamic structure factor $\mathscr{S}(q, \omega)$ from the MD simulation data, which requires the computation of some 10^4 time correlation functions. In the second step a Monte Carlo (MC) simulation of multiple scattering and absorption of neutrons in the sample has to be appended, taking $\mathscr{S}(q, \omega)$ from the MD simulation as input. The second step is necessary, since, even if multiple scattering is reduced by experimental means, it can still be 20–30% of the total scattering intensity.

In this paper we present simulations of inelastic neutron scattering spectra of CH_2Cl_2. We use the experimental data of Brier and Perry [2] as reference, since they are suited with respect to (1) and (2). The details of the MD simulations, in particular of the intermolecular MD potentials, are described in [1].

To calculate the dynamic structure factor, we apply the 'fast correlation algorithm' (FCA), which is based on the fast Fourier transform (FFT) and the Wiener–Khinchin theorem for discrete periodic functions. This algorithm is extremely fast on vector computers, if FFT routines are available that are specially designed for the vector-computer architecture.

2. The dynamic structure factor

2.1. *Basic relations*

The differential neutron-scattering cross-section of molecular liquids can be written as follows, splitting the dynamic structure factor $\mathscr{S}(q, \omega)$ into its *coherent* and *incoherent* parts:

$$\frac{d^2\sigma}{d\Omega\, dE} = N \frac{k}{k_0} [\mathscr{S}_{coh}(q, \omega) + \mathscr{S}_{inc}(q, \omega)]. \tag{3}$$

The energy transfer in the scattering process is given by $\hbar\omega = E_0 - E$, E_0 being the energy of the incident neutrons. Correspondingly, the momentum transfer is defined as $\hbar q = \hbar |\mathbf{k}_0 - \mathbf{k}|$. The coherent and incoherent dynamic structure factors are given by

$$\mathscr{S}_{coh}(q, \omega) = \frac{1}{2\pi\hbar} \int_{-\infty}^{\infty} dt\, e^{-i\omega t} \mathscr{F}_{coh}(q, t), \tag{4}$$

$$\mathscr{F}_{coh}(q, t) = \frac{1}{N} \sum_{\alpha, \beta} \sum_{i, j} \bar{b}_\alpha^* \bar{b}_\beta \langle e^{-i\mathbf{q} \cdot \mathbf{R}_{\alpha i}(0)}\, e^{i\mathbf{q} \cdot \mathbf{R}_{\beta j}(t)} \rangle, \tag{5}$$

$$\mathscr{S}_{inc}(q, \omega) = \frac{1}{2\pi\hbar} \int_{-\infty}^{\infty} dt\, e^{-i\omega t} \mathscr{F}_{inc}(q, t), \tag{6}$$

$$\mathscr{F}_{inc}(q, t) = \frac{1}{N} \sum_{\alpha, i} (\overline{|b_\alpha|^2} - |\bar{b}_\alpha|^2) \langle e^{-i\mathbf{q} \cdot \mathbf{R}_{\alpha i}(0)}\, e^{i\mathbf{q} \cdot \mathbf{R}_{\alpha i}(t)} \rangle. \tag{7}$$

The quantities $\mathscr{F}_{\mathrm{coh}}(q, t)$ and $\mathscr{F}_{\mathrm{inc}}(q, t)$ are the coherent and incoherent *intermediate scattering functions* respectively. Latin subscripts denote molecules and greek subscripts atoms in one molecule. The total number of atoms is $N = N_{\mathrm{m}} N_{\mathrm{a}}$, where N_{m} is the number of molecules and N_{a} the number of atoms in a single molecule. If we define $\mathrm{D}(\mathbf{q}, t)$ and $\mathrm{d}_{\alpha, i}(\mathbf{q}, t)$ to be the Fourier transforms of the weighted total particle density and the weighted single particle density,

$$\mathrm{D}(\mathbf{q}, t) = \frac{1}{N^{1/2}} \sum_{\alpha, i} \bar{b}_\alpha \, \mathrm{e}^{\mathrm{i}\mathbf{q} \cdot \mathbf{R}_{\alpha i}(t)}, \tag{8}$$

$$\mathrm{d}_{\alpha, i}(\mathbf{q}, t) = (\overline{|b_\alpha|^2} - |\overline{b_\alpha}|^2)^{1/2} \, \mathrm{e}^{\mathrm{i}\mathbf{q} \cdot \mathbf{R}_{\alpha i}(t)}, \tag{9}$$

then the coherent and incoherent intermediate scattering function can be written as

$$\mathscr{F}_{\mathrm{coh}}(\mathbf{q}, t) = \langle \mathrm{D}(-\mathbf{q}, 0) \mathrm{D}(\mathbf{q}, t) \rangle, \tag{10}$$

$$\mathscr{F}_{\mathrm{inc}}(\mathbf{q}, t) = \frac{1}{N} \sum_{\alpha, i} \langle \mathrm{d}_{\alpha, i}(-\mathbf{q}, 0) \mathrm{d}_{\alpha, i}(\mathbf{q}, t) \rangle. \tag{11}$$

The thermal averages $\langle \ldots \rangle$ stand for $Z^{-1} \, \mathrm{tr} \{ \mathrm{e}^{-\beta \mathrm{H}} \ldots \}$, where $Z = \mathrm{tr} \{ \mathrm{e}^{-\beta \mathrm{H}} \}$ and $\beta = 1/k_{\mathrm{B}} T$. To calculate the dynamic structure factor from MD simulations, the quantum-mechanical thermal averages given above are approximated by *time averages* over the MD trajectories, generated according to the laws of classical mechanics. In this picture the particle densities are no longer operators but rather ordinary functions depending on the positions of the atoms. We see from (10) and (11) that the coherent part of the intermediate scattering function is a single q-dependent time correlation function, whereas the incoherent part is the average over N q-dependent time correlation functions. Because all atoms labelled by α, i with α fixed and i running over all molecules are physically equivalent, $\mathscr{F}_{\mathrm{inc}}(\mathbf{q}, t)$ can be written as

$$\mathscr{F}_{\mathrm{inc}}(\mathbf{q}, t) = \frac{1}{N_{\mathrm{a}}} \sum_{\alpha} \langle d_{\alpha, 1}(-\mathbf{q}, 0) d_{\alpha, 1}(\mathbf{q}, t) \rangle, \tag{12}$$

summing only over the atoms of an arbitrary tagged molecule. From the computational point of view it is better to use (11), since averaging over all equivalent atoms reduces the statistical error considerably.

A fundamental relation that is fulfilled by the dynamic structure factor is the *relation of detailed balance* [3, 4]:

$$\mathscr{S}(q, \omega) = \mathrm{e}^{\beta \hbar \omega} \mathscr{S}(q, -\omega). \tag{13}$$

As an immediate consequence, the even and odd parts of $\mathscr{S}(q, \omega)$, given by

$$\mathscr{S}^{(+)}(q, \omega) = \tfrac{1}{2}(1 + \mathrm{e}^{-\beta \hbar \omega}) \mathscr{S}(q, \omega), \tag{14}$$

$$\mathscr{S}^{(-)}(q, \omega) = \tfrac{1}{2}(1 - \mathrm{e}^{-\beta \hbar \omega}) \mathscr{S}(q, \omega), \tag{15}$$

are related by

$$\mathscr{S}^{(-)}(q, \omega) = \tanh(\tfrac{1}{2} \beta \hbar \omega) \mathscr{S}^{(+)}(q, \omega). \tag{16}$$

In the classical limit ($\hbar \to 0$) the dynamic structure factor is an *even* function in ω [5] and all odd moments of $\mathscr{S}(q, \omega)$, defined by

$$\langle \omega^{2n+1} \rangle \equiv \int_{-\infty}^{\infty} \mathrm{d}\omega \, \omega^{2n+1} \mathscr{S}(q, \omega), \tag{17}$$

vanish. In this context we refer to a publication of Van Hove [6] in which it is shown that the imaginary part of the correlation function $\mathcal{G}(r, t)$, defined as the Fourier transform of the dynamic structure factor with respect to time and space, can be related to the local disturbance of the microscopic particle density caused by the neutron during the scattering process. In the classical limit $\mathcal{G}(r, t)$ is a *real* even function in t, and consequently $\mathcal{S}(q, \omega)$ is an even function in ω. We see that calculating the dynamic structure factor according to classical mechanics means neglecting the influence of the neutron on the target during the scattering process.

To correct a dynamic structure factor $\mathcal{S}_{\mathrm{cl}}(q, \omega)$ that has been calculated from a classical ensemble or time average for detailed balance, several *semiclassical correction methods* have been proposed [7–9]. The most common method is that of Schofield [7]:

$$\mathcal{S}(q, \omega) = \mathrm{e}^{\beta\hbar\omega/2}\mathcal{S}_{\mathrm{cl}}(q, \omega), \tag{18}$$

$$\mathcal{F}(q, t) = \mathcal{F}_{\mathrm{cl}}(q, t - \tfrac{1}{2}\mathrm{i}\beta\hbar). \tag{19}$$

We used the method of Lovesey [4], which is also easy to implement:

$$\mathcal{S}(q, \omega) = \frac{\beta\hbar\omega}{1 - \mathrm{e}^{-\beta\hbar\omega}}\,\mathcal{S}_{\mathrm{cl}}(q, \omega), \tag{20}$$

$$\mathcal{F}(q, t) - \mathcal{F}(q, -t) = -\mathrm{i}\beta\hbar\,\frac{\partial}{\partial t}\,\mathcal{F}_{\mathrm{cl}}(q, t). \tag{21}$$

This correction method has the advantage that at least the first moment, called the recoil moment, of the corrected dynamic structure factor is exact, whereas Schofield's correction method yields a recoil moment that is only correct up to first order in $\hbar$ [10]. The recoil moment does not depend on the interaction potentials between the molecules and is equal to the energy transferred from the neutron to the target in a scattering process, if the target is at rest before the collision. Both semiclassical correction methods, by construction, ensure detailed balance of the corrected dynamic structure factor and are valid in the (q, ω) region given in (1) and (2) [10].

2.2. *Efficient calculation of the dynamic structure factor from MD simulations*

We now discuss the efficient calculation of the dynamic structure factor $\mathcal{S}_{\mathrm{cl}}(q, \omega)$ from MD simulations. As is clear from (11), the most time-consuming part is the calculation of the incoherent intermediate scattering function, since we have to average over $N \approx 100$–1000 single-particle density correlation functions to obtain maximum statistical accuracy.

The general scheme for the calculation of $\mathcal{F}_{\mathrm{coh}}(q, t)$ from MD simulations has already been given in [1] in the context of the computation of the coherent intermolecular structure factor from the Fourier-transformed particle density ('direct method'). The same scheme applies to the computation of $\mathcal{F}_{\mathrm{inc}}(q, t)$—merely an additional averaging over the single-particle correlation functions has to be performed. If N_t is the number of MD configurations on the *equidistant* discrete time scale $t = m\,\Delta t$, given by the MD simulation, then we write explicitly, abbreviating $m\,\Delta t$ by m etc.,

$$\mathcal{F}_{\mathrm{coh}}(\mathbf{q}, m) \approx \langle D(-\mathbf{q}, 0)D(\mathbf{q}, m)\rangle_{\mathrm{cl}}$$

$$= \frac{1}{N_t - m}\sum_{k=0}^{N_t - m - 1} D(-\mathbf{q}, k)D(\mathbf{q}, k + m), \tag{22}$$

$$\mathscr{F}_{\mathrm{inc}}(\mathbf{q}, m) \approx \frac{1}{N} \sum_{\alpha, i} \langle d_{\alpha, i}(-\mathbf{q}, 0) d_{\alpha, i}(\mathbf{q}, t) \rangle_{\mathrm{cl}}$$

$$= \frac{1}{N} \sum_{\alpha, i} \left[\frac{1}{N_t - m} \sum_{k=0}^{N_t - m - 1} d_{\alpha, i}(-\mathbf{q}, k) d_{\alpha, i}(\mathbf{q}, k + m) \right]. \tag{23}$$

The index m runs from 0 to $N_t - 1$, and we have $\mathscr{F}(\mathbf{q}, m) = \mathscr{F}(-\mathbf{q}, |m|)$ for $m \in [-N_t + 1, -1]$. To calculate the discrete-time correlation functions, one can make use of the discrete form of the *Wiener–Khinchin theorem* [11]:

For an arbitrary complex discrete signal $u(k)$, $k \in [0, N_t - 1]$, the estimate $C_{uu}(m)$ of its time autocorrelation function, defined by

$$C_{uu}(m) = \begin{cases} \dfrac{1}{N_t - m} \displaystyle\sum_{k=0}^{N_t - m - 1} u^*(k) u(k + m) & \text{for } m \in [0, N_t - 1], \\ C_{uu}^*(|m|), & \text{for } m \in [-N_t + 1, -1], \end{cases} \tag{24}$$

can be written in the form, for $m \in [-N_t + 1, N_t - 1]$,

$$C_{uu}(m) = \frac{1}{N_t - |m|} \frac{1}{2N_t} \sum_{n=0}^{2N_t - 1} \exp\left(\mathrm{i} \frac{2\pi}{2N_t} mn \right) |\hat{U}(n)|^2, \tag{25}$$

where

$$\hat{U}(n) \equiv \sum_{k=0}^{2N_t - 1} \exp\left(-\mathrm{i} \frac{2\pi}{2N_t} nk \right) U(k) \tag{26}$$

is the discrete Fourier transform of the function $U(k)$, which is identical with $u(k)$ for $k \in [0, N_t - 1]$, but padded with N_t zeros, i.e. $U(k) = 0$ for $k \in [N_t, 2N_t - 1]$.

Since $u(k)$ has to be regarded as an equidistant sampled signal of *finite* length of a function $u(t)$, $t \in [-\infty, +\infty]$, the zero-padding in $U(k)$ is necessary to avoid spurious correlations. With respect to (22) and (23), the finite length is simply given by the length of the simulation run. It should be remarked that $U(k)$ and $\hat{U}(n)$ are periodic with period $2N_t$.

If the fast-Fourier-transform algorithm (FFT) is used to perform the discrete forward and backward Fourier transform in (25), one obtains a speed up of $O(2N_t \log_2 2N_t)$ operations (multiplications) against $O(N_t^2)$ operations required for the direct method according to (24). This method is usually referred to as *fast correlation algorithm* (FCA). The use of highly vectorized assembler routines for FFTs on vector computers gives an additional improvement—in the case of a Cray XM-P an additional speed-up factor of approximately 5–7 [10]. Despite the fact that the FCA is well known (see e.g. [12]), and also that some publications in the field of molecular dynamics have pointed out its usefulness [13–15], it is not a common tool in the analysis of MD simulations. We emphasize that (25) expresses a mathematical identity and does not involve any 'truncation errors'—it is merely another way of writing $C_{uu}(m)$, and can be used to calculate time correlation functions efficiently. To handle the input/output for the application of the FCA in a convenient manner, we have developed a small package of subroutines that makes it possible to treat large datasets as 'matrices', with buffered I/O operations on 'rows' (e.g. coordinates/velocities of *all* particles at *one* time step) and 'columns' (e.g. the coordinates/velocities of *one* particle at *all* time steps) [10].

Although (25) shows that the power spectrum of the input signal $u(k)$ could be

estimated by $|\hat{U}(n)|^2$, for all practical purposes spectral smoothing has to be performed. This means that (25) has to be used only as a 'trick' to calculate correlation functions efficiently, and spectral smoothing has to be performed afterwards in a separate process. We did this by multiplying the incoherent scattering functions by a Gauss window [16] before performing the Fourier transform to get the corresponding dynamic structure factors according to (4) and (6).

3. Multiple scattering

Quantitative comparison between dynamic structure factors from neutron-scattering experiments and MD simulations requires consideration of the effect of multiple scattering and absorption in macroscopic specimens. It is well known that multiple-scattering intensities in *inelastic* neutron experiments are strongly dependent on the energy transfer between neutron and target and in principal cannot be subtracted from the measured neutron spectrum without knowing the dynamic structure factor, the quantity of interest itself [17–19]. To compare with the experimental data of Brier and Perry [2], we decided to take the total dynamic structure factor $\mathcal{S}(q, \omega) = \mathcal{S}_{\text{coh}}(q, \omega) + \mathcal{S}_{\text{inc}}(q, \omega)$ from the MD simulation as input for an additional simulation of multiple-scattering and absorption effects, after applying the semiclassical correction formula (20). In an analogous manner the comparison between theoretical models for $\mathcal{S}(q, \omega)$ and experimental data in [2] has been done.

We used the following approach to perform the simulations of multiple scattering and absorption [10]. Starting from the differential cross-section for inelastic neutron scattering given by (3), we rewrite it for the scattering process from a volume element d^3r in the form

$$\frac{\mathrm{d}^2\sigma}{\mathrm{d}\Omega\,\mathrm{d}E} = \rho\,\mathrm{d}^3r\,\frac{k}{k_0}\,\mathcal{S}(q, \omega), \tag{27}$$

where ρ is the average density of scatterers in the specimen and $(k/k_0)\mathcal{S}(q, \omega)$ is simply the average differential scattering cross-section per atom in a small volume element. The energy and momentum transfer are given by $\hbar\omega = E_0 - E$ and $\hbar q = \hbar|\mathbf{k}_0 - \mathbf{k}|$.

We now look at single scattering from a volume element d^3r_1, located at $\mathbf{r}_1$ in a macroscopic specimen. The number of neutrons scattered from this volume element into a solid-angle element $\mathrm{d}\Omega$ and an energy interval $\mathrm{d}E$ around Ω and E is given by

$$\mathrm{d}I^{(1)}(\Omega, E; \mathbf{r}_1) = \rho\,\mathrm{d}^3r_1\,j_{\text{in}}(\mathbf{k}_0; \mathbf{r}_1)\,\frac{k}{k_0}\,\mathcal{S}(q, \omega)\,\mathrm{e}^{-\mu(E)r_{1B}}\,\mathrm{d}\Omega\,\mathrm{d}E, \tag{28}$$

$$j_{\text{in}}(\mathbf{k}_0; \mathbf{r}_1) = j_0\,\mathrm{e}^{-\mu(E_0)r_{01}}, \tag{29}$$

where we denote by $j_{\text{in}}(\mathbf{k}_0; \mathbf{r}_1)$ the current density of the unscattered neutrons in the direction of $\mathbf{k}_0$ at the location $\mathbf{r}_1$ of the volume element under consideration. The energy-dependent absorption coefficient $\mu(E)$ is defined by $\mu(E) \equiv \rho[\Sigma_s(E) + \Sigma_r(E)]$, where $\Sigma_s(E)$ is the total scattering cross-section and $\Sigma_r(E)$ the reaction cross-section. For the reaction cross-section the relation $\Sigma_r(E) \propto E^{-1/2}$ usually holds. The distances r_{01} and r_{1B} are the distances between entry point and scattering volume and between scattering volume and exit point of the neutrons. It should be noted that Ω describes the flight direction of the scattered neutrons with respect to $\mathbf{k}_0$. The total differential scattering cross-section of the macroscopic specimen for single

scattering is obtained from (28) and (29) by integration over the volume of the specimen and normalizing the result to j_0, $d\Omega$ and dE:

$$\frac{d^2\sigma^{(1)}}{d\Omega\, dE} = \rho \frac{k}{k_0} \int_V d^3r_1\, e^{-\mu(E_0)(r_{01}+r_{1B})} S^{(1)}(\Omega, E \mid \mathbf{r}_1), \tag{30}$$

$$S^{(1)}(\Omega, E \mid \mathbf{r}_1) = \mathscr{S}(q, \omega)\, e^{-\Delta\mu(E) r_{1B}}, \tag{31}$$

with $\Delta\mu(E) \equiv \mu(E) - \mu(E_0)$.

Analogously to single scattering, we write for the number of neutrons scattered first at a volume element d^3r_1, located at $\mathbf{r}_1$, and then at a second volume element d^3r_2, located at $\mathbf{r}_2$, the following:

$$dI^{(2)}(\Omega, E; \mathbf{r}_1, \mathbf{r}_2) = \rho\, d^3r_2\, j_{in}(\mathbf{k}_1; \mathbf{r}_1, \mathbf{r}_2) \frac{k}{k_1} \mathscr{S}(q_2, \omega_2)\, e^{-\mu(E) r_{2B}}\, d\Omega\, dE, \tag{32}$$

$$j_{in}(\mathbf{k}_1; \mathbf{r}_1, \mathbf{r}_2) = \rho\, d^3r_1\, j_{in}(\mathbf{k}_0; \mathbf{r}_1) \frac{k_1}{k_0} \mathscr{S}(q_1, \omega_1) \frac{e^{-\mu(E_1) r_{12}}}{r_{12}^2} \hbar\, d\omega_1. \tag{33}$$

The momentum transfers are given by $\hbar q_1 = \hbar |\mathbf{k}_0 - \mathbf{k}_1|$, $\hbar q_2 = \hbar |\mathbf{k}_1 - \mathbf{k}|$, and the energy transfers by $\hbar\omega_1 = E_0 - E_1$, $\hbar\omega_2 = E_1 - E$. Apart from the damping factor $e^{-\Delta\mu(E_1) r_{12}}$, (33) follows from elementary scattering theory [4], taking the current density of the neutrons scattered from volume element d^3r_1 as input current density for the second scattering event. The incoherent superposition of the current densities is valid under the assumption that the mean free path $\bar{\lambda}$ of the neutrons is much larger than their coherence length λ_c. This is a reasonable assumption since $\bar{\lambda}$ is of the order of a few millimetres whereas λ_c is of the order of 100 Å.

To obtain the differential cross-section for double scattering, we switch from the integration variables $\mathbf{r}_1$ and $\mathbf{r}_2$ to $\mathbf{r}_1$ and $\mathbf{r}_{12} = \mathbf{r}_2 - \mathbf{r}_1$, and use spherical polar coordinates for the integration over $\mathbf{r}_{12}$. With the same normalization as in the case of single scattering, we obtain

$$\frac{d^2\sigma^{(2)}}{d\Omega\, dE} = \rho^2 \frac{k}{k_0} \int_V \int_0^{L_{12}} \int_{4\pi} d^3r_1\, dr_{12}\, d\Omega_{12}$$
$$e^{-\mu(E_0)(r_{01}+r_{12}+r_{2B})} S^{(2)}(\Omega, E \mid \mathbf{r}_1, r_{12}, \Omega_{12}), \tag{34}$$

$$S^{(2)}(\Omega, E \mid \mathbf{r}_1, r_{12}, \Omega_{12}) = \hbar \int_{-\infty}^{E_0/\hbar} d\omega_1 \mathscr{S}(q_1, \omega_1) S(q_2, \omega_2)\, e^{-[\Delta\mu(E_1) r_{12} + \Delta\mu(E) r_{2B}]}. \tag{35}$$

The upper limit L_{12} on the integration over r_{12} is the distance between $\mathbf{r}_1$ and the boundary of the specimen in the direction of $\mathbf{r}_{12}$. Expressions for higher-order multiple-scattering cross-sections can be obtained by straightforward generalization of (34) and (35). In this work we have neglected multiple scattering for orders higher than two. It should be noted that in the case of isotropic and elastic scattering, expressed by the relation $\mathscr{S}(q, \omega) = b^2\delta(\hbar\omega)$ (b is the average incoherent scattering length of the scatterers), the expression for the relation between double and single scattering of Blech and Averbach [20] can be retrieved from (30), (31) and (34), (35).

To perform the numerical calculation of inelastic multiple-scattering intensities, we used a Monte Carlo (MC) method for the space integrations and a conventional 'exact' numerical integration method on a non-equidistant grid for the integration over the intermediate energy transfer $\hbar\omega_1$ in (35). In this way the MC integration error with respect to $\hbar\omega_1$ could be eliminated. The distribution of the grid points

was chosen according to a Lorentz distribution, with a high density of grid points in the quasi-elastic region and a lower density in the inelastic region where the dynamic structure varies only very slowly [10]. The integration over Ω_{12} was performed by importance sampling, using a distribution function proportional to $\int_{-\infty}^{\infty} d\omega S(q(\theta, \omega = 0), \omega)$.

4. Results and discussion

As already mentioned in section 1, we have chosen the inelastic neutron-scattering intensities published by Brier and Perry [2] as reference data for our *simulated scattering* intensities of CH_2Cl_2. The experimental data are *time-of-flight* (TOF) spectra, obtained from the IN5 spectrometer at the high-flux reactor of the Institut Laue-Langevin, Grenoble, France. We report the most important parameters of the experimental setup according to [2]:

(i) the energy of the incident neutrons E_0 was 1·326 meV, which corresponds to a wavelength of $\lambda_0 = 8$ Å and a time of flight $\tau_0 = 2055\,\mu s\,m^{-1}$;

(ii) the energy resolution ΔE was 50 μeV (full width at half-maximum);

(iii) (*sample geometry*) the sample was contained in a thin-walled (0·05 cm) aluminium cell of 5 cm × 5 cm area and 0·032 cm thickness, excluding the walls;

(iv) (*orientation of sample*) the sample was set at 45° with respect to the incident neutron beam, and the experiment was performed in transmission geometry;

(v) the detector angles were 35°, 53·8°, 73° and 88·4°.

To calculate the high-resolution scattering intensities from MD trajectories, we performed a MD simulation of 320 ps real time—corresponding to 65 536 steps of 5 fs—for a system of 108 CH_2Cl_2 molecules in a cubic simulation box of 22·56 Å box length. The details of the MD simulation are presented in section 2 of [1]. As in [1] the MD potentials that we used for our simulations are those of Ferrario and Evans, referred to as (A) [21], and Böhm and Ahlrichs, referred to as (B) [22]. The analysis file contained 8192 configurations with a time distance of eight MD steps, i.e. 40 fs. In this way a resolution $\Delta E = 6{\cdot}3\,\mu eV$ in the unsmoothed dynamic structure factor could be obtained. The maximum energy transfer accessible according to time distance of the dumped configurations is $\hbar\omega_{max} = 100$ meV, corresponding to a TOF of $225\,\mu s\,m^{-1}$. To smooth the dynamic structure factor, we used a Gauss window [16] with exactly the same spectral resolution as in the experimental data.

The neutron-scattering intensities presented by Brier and Perry [2] are corrected for the detector efficiency, but *not* for multiple scattering and absorption. To compare our simulated scattering intensities with the experimental data, we performed the simulation of multiple scattering and absorption as described in section 3. The actual calculation was done with the program MSDYN2 [10]. Since the flux of the incident neutrons is not given in [2], the comparison between experiment and simulation was done on an arbitrary intensity scale. We scaled the intensities in such a way that the quasi-elastic peaks had the same height. Concerning the representation of the TOF-spectra in figures 1–4, it should be noted that the conversion of the inelastic scattering intensities from the (Θ, ω) scale to the (Θ, τ) scale has to be performed using the formula

$$\frac{d^2\sigma}{d\Omega\, d\tau} \propto E^{3/2} \frac{d^2\sigma}{d\Omega\, dE}, \tag{36}$$

$$E = \tfrac{1}{2}m\tau^{-2}. \tag{37}$$

If the time of flight τ is measured in $\mu s\,m^{-1}$ and the energy $E = E_0 - \hbar\omega$ in meV, the conversion from the energy scale to the TOF scale is made using $\tau = 2285E^{-1/2}$.

We see from figures 1–4 that the simulated TOF spectra are qualitatively correct for both MD potentials. However, both potentials underestimate the intensities in the region of inelastic scattering, corresponding to shorter flight times, and the width of the quasi-elastic line for higher detector angles. It is obvious that multiple-scattering effects have to be considered in order to make quantitative comparisons between experiment and simulation.

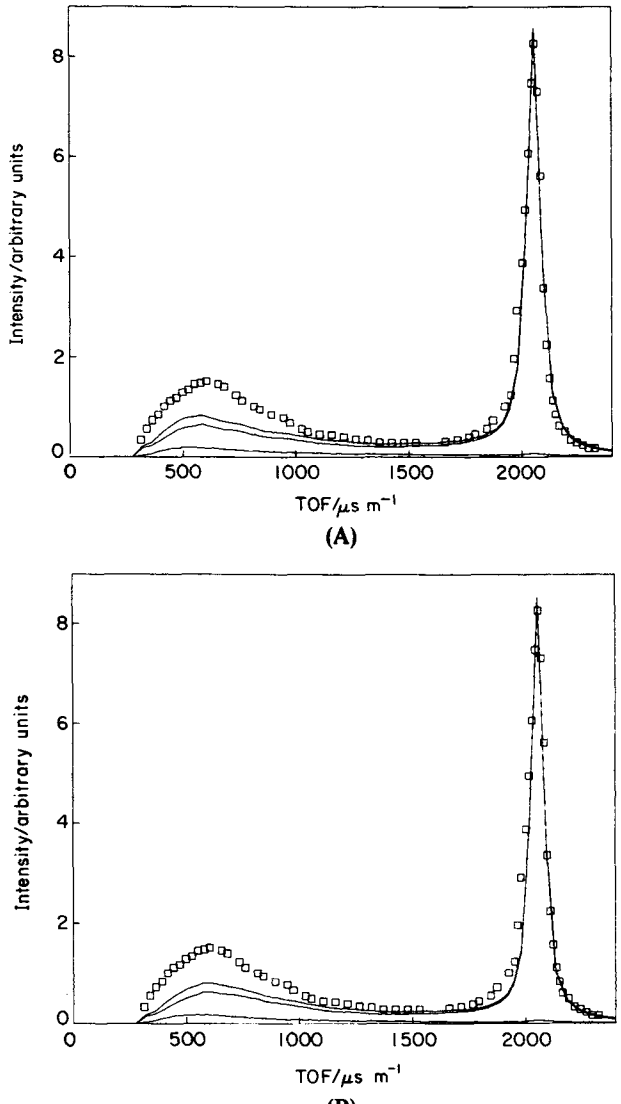

Figure 1. Experimental and simulated TOF spectra for $\Theta = 35{\cdot}0°$. (A) and (B) refer to the MD potentials of Ferrario and Evans [21] and Böhm and Ahlrichs [22] respectively. Squares are experimental points; solid lines represent from top to bottom, total, single and double scattering intensity.

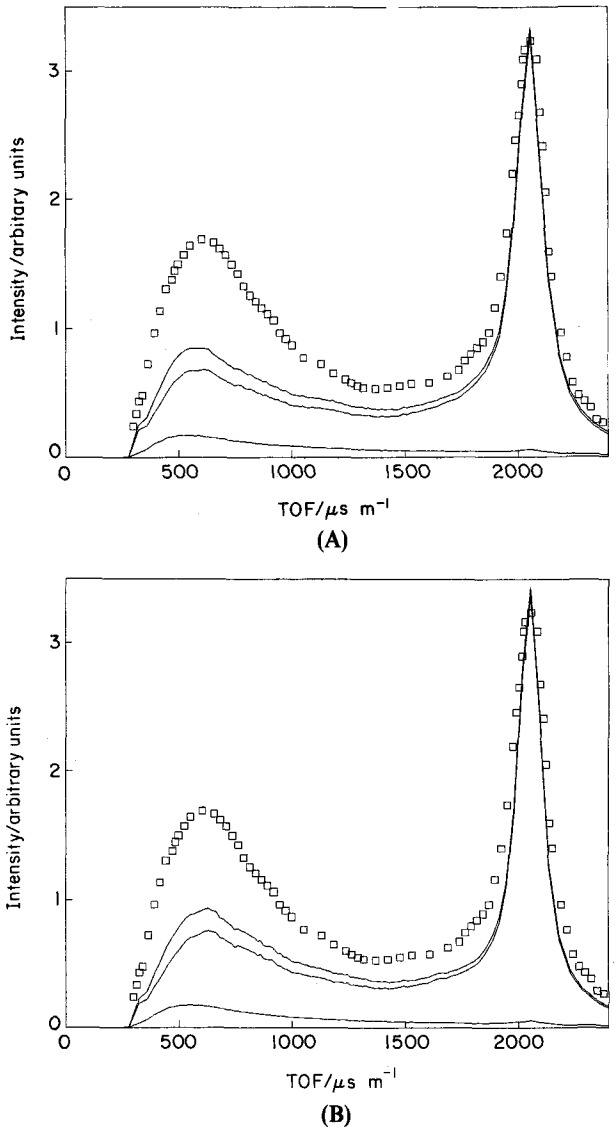

Figure 2. As figure 1, but for $\Theta = 53{\cdot}8°$.

The discrepancy between simulated and experimental spectra in the inelastic region is probably due to the fact that for the simulated liquids the 'cage' of nearest neighbours in which a central molecule performs strongly damped oscillatory motions is not as stable as in the real liquid. The cage effect produces the characteristic overdamped oscillations of the VACFs shown in figure 5, which is reflected in the broad frequency band between about 2 meV and about 20 meV in their Fourier transforms (see figure 6). This frequency interval can be converted into $500\,\mu s\,m^{-1} \leqslant \tau \leqslant 1600\,\mu s\,m^{-1}$. We should point out that comparison between the Fourier transforms of the single-atom VACFs and the TOF scattering intensities is quite straightforward, since, owing to the anomalously high incoherent scattering cross-section of the hydrogens, we have approximately [23] (see figure 7):

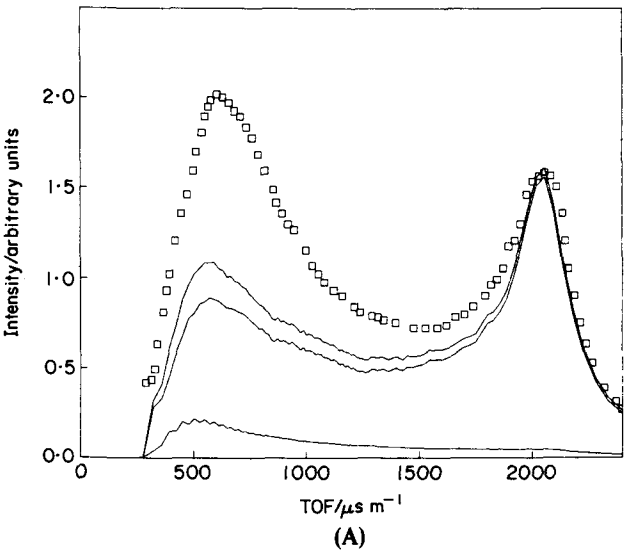

(A)

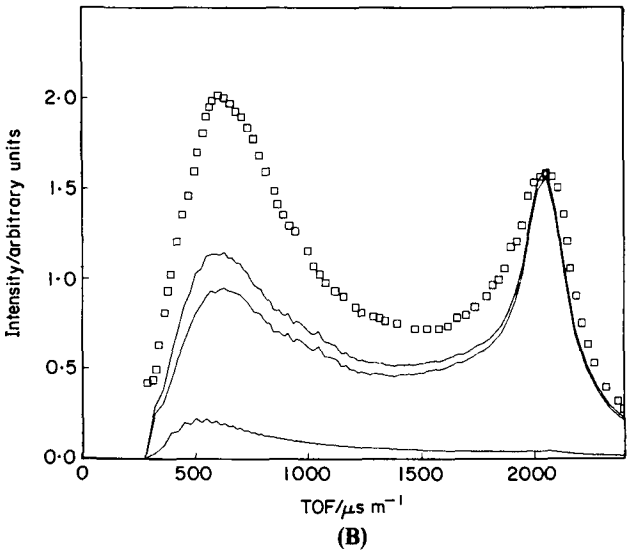

(B)

Figure 3. As figure 1, but for $\Theta = 73{\cdot}0°$.

$$\lim_{q\to 0} \frac{\omega^2}{q^2} \mathscr{S}_{\text{inc}}(q, \omega) \propto \int_{-\infty}^{+\infty} \mathrm{d}t\, \mathrm{e}^{\mathrm{i}\omega t} \langle \mathbf{v}_{\mathrm{H}}(0) \cdot \mathbf{v}_{\mathrm{H}}(t) \rangle. \tag{38}$$

Because of (36) and (3), we get for $E \gg E_0$ or $\omega \approx -E/\hbar$

$$\frac{\mathrm{d}^2\sigma}{\mathrm{d}\Omega\, \mathrm{d}\tau} \propto \omega^2 \mathscr{S}_{\text{inc}}(q, \omega). \tag{39}$$

It should be kept in mind that the momentum transfer is a function of the energy E for a given scattering angle Θ, which can be approximated for $E \gg E_0$ by

$$q \approx \frac{0{\cdot}6945 E^{1/2}}{1 + (E_0/E)^{1/2} \cos \Theta}, \tag{40}$$

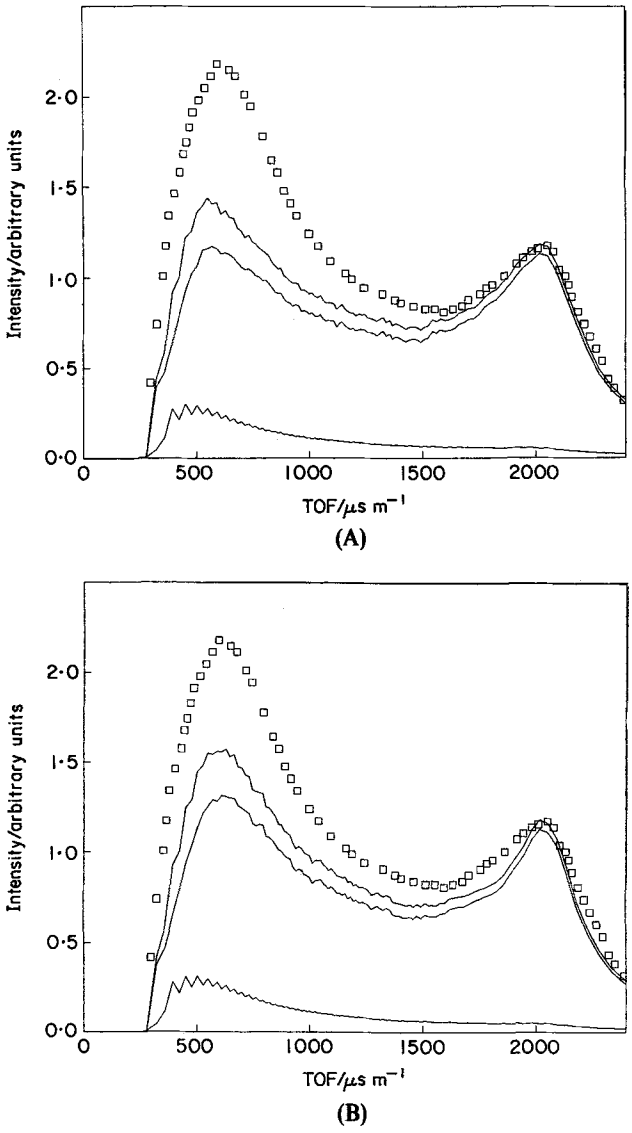

Figure 4. As figure 1, but for $\Theta = 88{\cdot}4°$.

if q is measured in Å^{-1} and E in meV. Comparison between the scattering intensities produced with potentials (A) and (B) shows that the B intensities are a little bit closer to reality in the inelastic region, which in fact is reflected in a narrower frequency band in the spectra of the hydrogen VACFs and therefore a more pronounced cage effect. We emphasize that intramolecular vibrations can be neglected in the (q, ω) region covered by the experiment of Brier and Perry [2] since we have approximately the following bounds for the relevant contributions to the scattering intensities: $0\,\text{Å} < q < 5\,\text{Å}^{-1}$ and $|\hbar\omega| < 30\,\text{meV}$. Therefore the Debye–Waller factors are in good approximation equal to one [2], and we have no vibrational contributions in the spectrum, because the lowest frequency from intramolecular vibrations can be seen at $\omega = 35{\cdot}1$ meV [24].

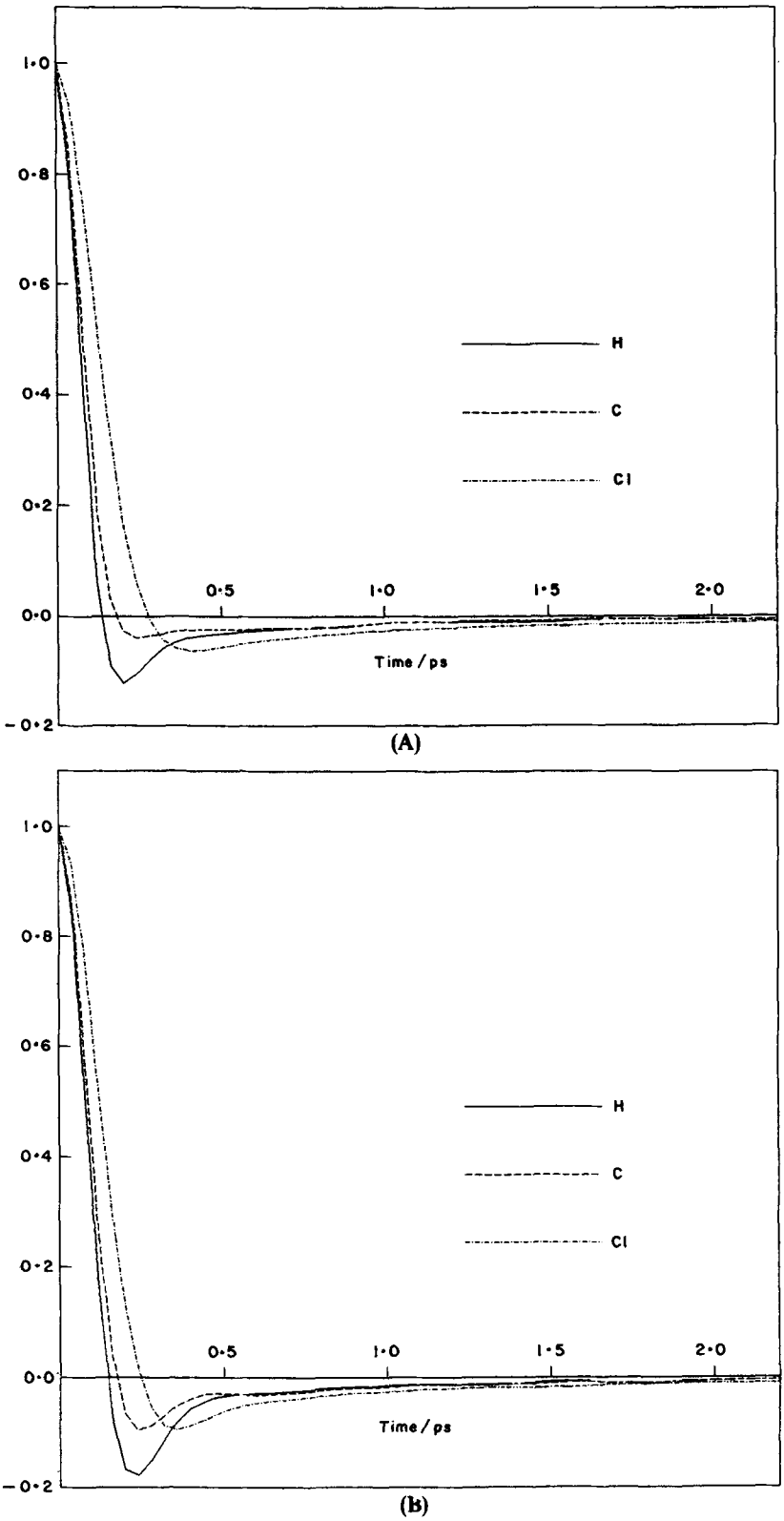

Figure 5. Single-atom velocity autocorrelation functions. (A) and (B) refer to the MD potentials of Ferrario and Evans [21] and Böhm and Ahlrichs [22] respectively.

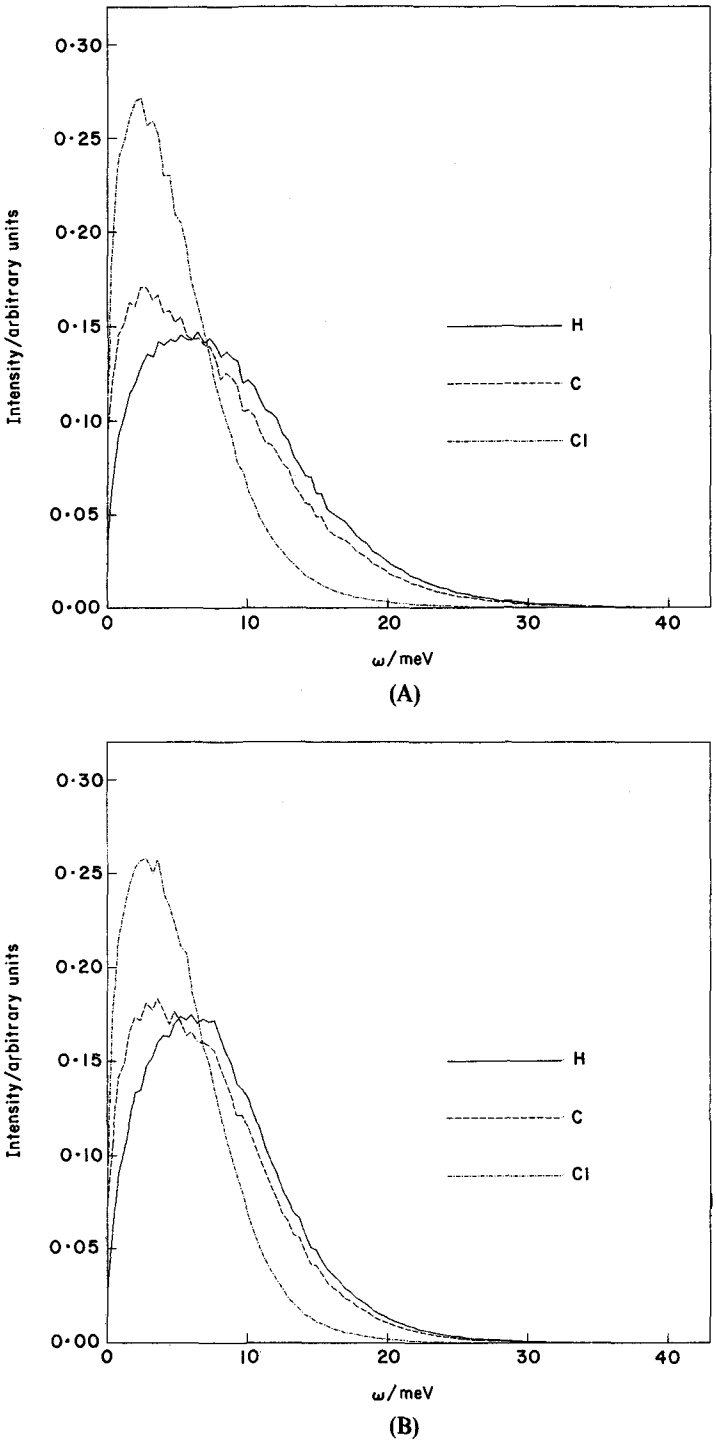

Figure 6. Power spectra of single-atom velocities. (A) and (B) refer to the MD potentials of Ferrario and Evans [21] and Böhm and Ahlrichs [22] respectively.

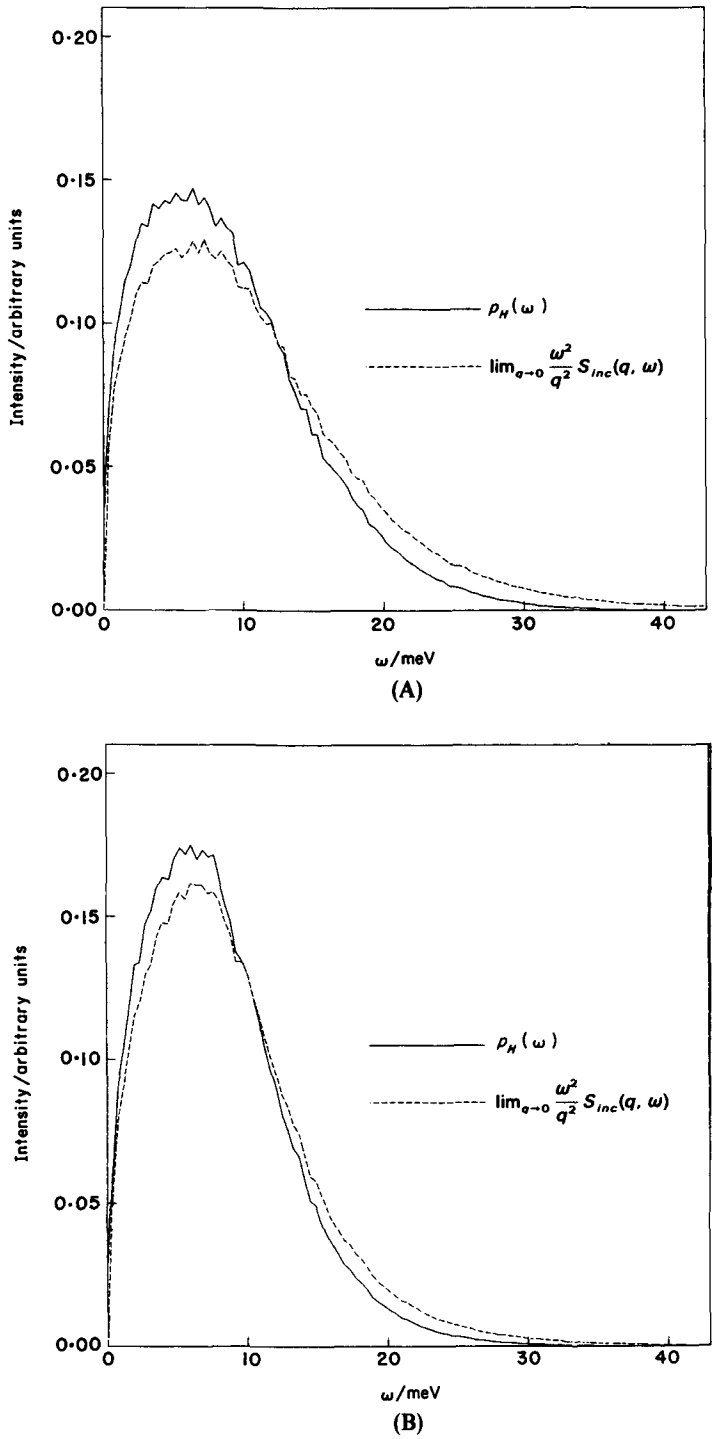

Figure 7. Incoherent dynamic structure factor and power spectrum of hydrogen velocities. The limit $q \to 0$ is approximated by taking the smallest possible value for q, given by $q = 2\pi/L = 0{\cdot}278\,\text{Å}^{-1}$, where L is the size of the MD box. (A) and (B) refer to the MD potentials of Ferrario and Evans [21] and Böhm and Ahlrichs [22] respectively.

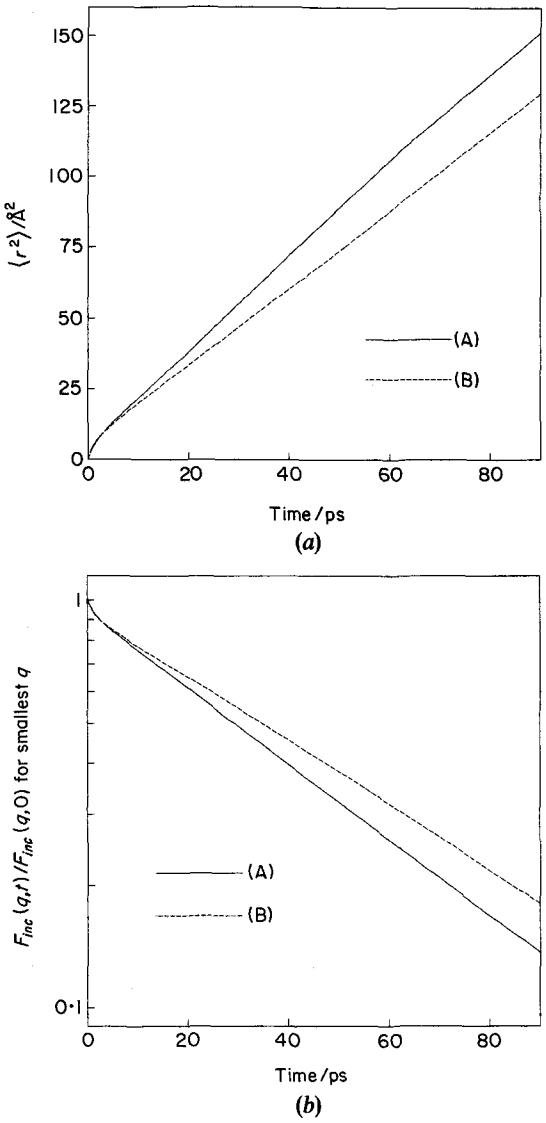

Figure 8. Mean-square displacement $\langle r^2 \rangle(t)$ of hydrogen (*a*) and incoherent intermediate scattering function $\mathscr{F}_{inc}(q, t)/\mathscr{F}_{inc}(q, 0)$ (*b*). (A) and (B) refer to the MD potentials of Ferrario and Evans [21] and Böhm and Ahlrichs [22] respectively.

Looking at the quasi-elastic lines of the simulated spectra at $\Theta = 35°$ or $q \approx 0{\cdot}5\,Å^{-1}$, where it is almost only *translational* diffusion that can be seen, we find the quasi-elastic line reproduced quite well by both potentials. Brier and Perry [2] find a diffusion coefficient of $3{\cdot}3 \times 10^{-5}\,cm^2\,s^{-1}$ by deconvolution of the measured spectrum. We calculated the translational diffusion coefficient D_t from the mean-square displacement of the hydrogens and from the incoherent intermediate scattering function for the smallest q vector (figure 8), using the fact that, to a very good approximation, $\mathscr{F}_{inc}(q, t) \propto e^{-D_t q^2 t}$. We find consistently $D_t = 2{\cdot}7(2{\cdot}8) \times 10^{-5}\,cm^2\,s^{-1}$ for potential A and $D_t = 2{\cdot}3(2{\cdot}4) \times 10^{-5}\,cm^2\,s^{-1}$ for potential B. The reason why the discrepancy with respect to the value found by Brier and Perry

[2] does not show up in different widths of the quasi-elastic lines is the influence of the spectral window. The latter has a width of 50 μeV, which is not small compared with the total width of the quasi-elastic line at $\Theta = 35°$. In this way, differences in the peak width are smoothed considerably by convolution of the 'ideal' quasi-elastic line with the spectral window. Diffusion coefficients for CH_2Cl_2 measured by NMR at $T = 300$ K are given in the literature: $D_t = 3{\cdot}8 \times 10^{-5}\,cm^2\,s^{-1}$ is found by Rothschild [25] and $D_t = 3{\cdot}7 \times 10^{-5}\,cm^2\,s^{-1}$ by O'Reilly [26].

At higher scattering angles and momentum transfers the deviation in the width of the quasi-elastic line between simulated and experimental spectra becomes more pronounced. Here the rotational diffusion is dominating. One finds consistently that the correlation time corresponding to one of the axis involving H atoms, the H–H

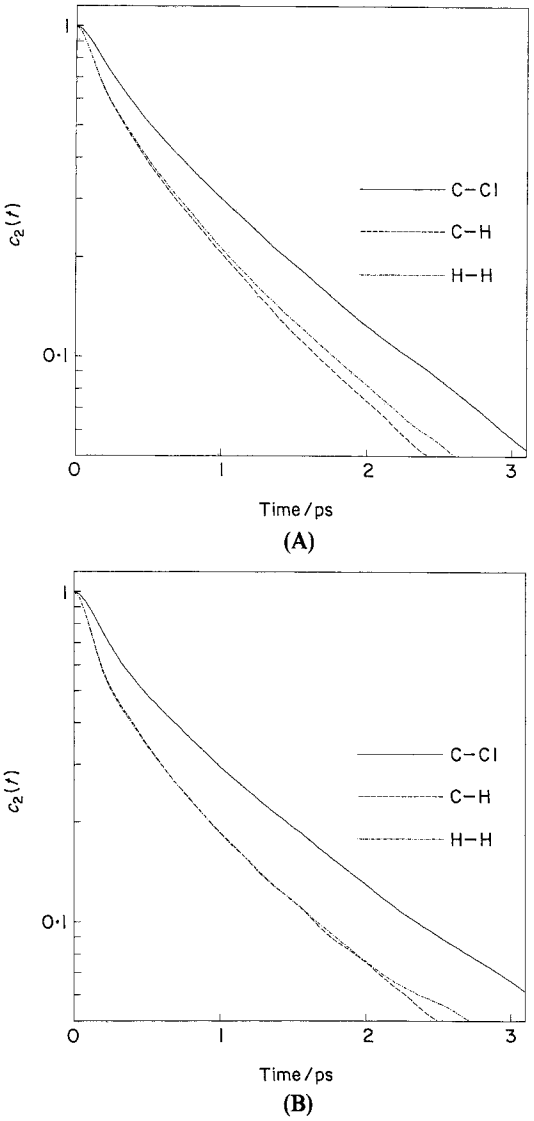

Figure 9. Reorientational correlation functions $c_2(t)$. (A) and (B) refer to the MD potentials of Ferrario and Evans [21] and Böhm and Ahlrichs [22] respectively.

vector axis, is larger than the value found from NMR (see the table—the experimental values are taken from [2]). We recall at this point that almost only the H atoms are 'seen' by the neutrons. The correlation times τ^∞ and τ in the table are defined by $1/\tau^\infty \equiv \lim_{t\to\infty} [-(\mathrm{d}/\mathrm{d}t) \ln c_2(t)]$ and $\tau \equiv \int_0^\infty \mathrm{d}t c_2(t)$, where the reorientational correlation function $c_2(t)$ is shown in figure 9. We conclude that both of the MD potentials used in our present work give a reasonable description of liquid CH_2Cl_2, especially concerning the structure, but have some deficiencies with respect to reproduction of its dynamic behaviour. The 'cage effect' and diffusive motion are underestimated.

Reorientational correlation times for CH_2Cl_2.

Axis	Potential	τ^∞/ps	τ/ps	τ_{NMR}/ps
C–Cl	(A)	1·22 ± 0·06	0·94 ± 0·05	1·20 ± 0·10
	(B)	1·32 ± 0·07	0·94 ± 0·05	1·20 ± 0·10
C–H	(A)	1·08 ± 0·05	0·68 ± 0·03	0·70 ± 0·07
	(B)	1·25 ± 0·06	0·67 ± 0·03	0·70 ± 0·07
H–H	(A)	1·13 ± 0·06	0·70 ± 0·04	0·53 ± 0·06
	(B)	1·35 ± 0·07	0·67 ± 0·03	0·53 ± 0·06

We gratefully acknowledge financial support from the Land Nordrhein-Westfalen and from the Bundesministerium für Forschung und Technologie (Project 03-ZE1AAC-0). Furthermore, we thank Professor Zeidler and Professor Bertagnolli for helpful discussions, and Professor Springer and the KFA Jülich for generous support with computer time.

References

[1] Kneller, G. R., and Geiger, A., 1989, *Molec. Phys.*, **68**, 487.
[2] Brier, W. G., and Perry, M. D., 1978, *Adv. Molec. rel. int. Proc.* **13**, 1.
[3] Turchin, V. F. 1965, *Slow Neutrons* (Israel Program for Scientific Translations).
[4] Lovesey, S. W., 1984, *Theory of Neutron Scattering from Condensed Matter*, Vol. 1 (Clarendon).
[5] Van Hove, L., 1954, *Phys. Rev.*, **95**, 249.
[6] Van Hove, L., 1958, *Physica*, **24**, 404.
[7] Schofield, P., 1960, *Phys. Rev. Lett.*, **4**, 239.
[8] Windsor, C. G., 1973, in *Chemical Applications of Thermal Neutron Scattering*, edited by B. T. M. Willis (Oxford University Press).
[9] Aamodt, R., Case, K. M., Rosenbaum, M., and Zweifel, P. F., 1962, *Phys. Rev.*, **126**, 1165.
[10] Kneller, G. R., 1988, PhD thesis, RWTH Aachen, and Report 2215, KFA Jülich (ISSN 0366-0885), Zentralbibliothek der Kernforschungsanlage Jülich, D-5170 Jülich, Postfach 1913.
[11] Reichl, L. E., 1980, *A Modern Course in Statistical Physics* (University of Texas Press).
[12] Brigham, E. O., 1974, *The Fast Fourier Transform* (Prentice-Hall).
[13] Kestamont, E., and Van Craen, J., 1976, *J. comput. Phys.*, **22**, 451.
[14] Smith, W., 1982, Information Quarterly for MD & MC Simulations, Daresbury Laboratory, U.K., No. 5, p. 34, and No. 7, p. 12.
[15] Fincham, D., Heyes, D. M., 1985, *Dynamical Processes in Condensed Matter*, edited by M. W. Evans (Wiley), p. 493.
[16] Harris, F. J., 1978, *Proc. Inst. elect. electron. Engrs*, **66**, 51.
[17] Brugger, R. M., 1968, *Nucl. Sci. Engng*, **33**, 187.

[18] SLAGGIE, E. L., 1969, *Nucl. Sci. Engng*, **36**, 105.
[19] SEARS, V. F., 1975, *Adv. Phys.*, **24**, 1.
[20] BLECH, I. A., and AVERBACH, B. L., 1965, *Phys. Rev.*, **137**, A1113.
[21] FERRARIO, M., and EVANS, M. W., 1982, *Adv. Molec. Relax. Int. Proc.*, **24**, 139. See also: EVANS, M. W., and EVANS, G. J., 1985, *Dynamical Processes in Condensed Matter*, edited by M. W. Evans (Wiley), p. 377.
[22] BÖHM, H. J., and AHLRICHS, R., 1985, *Molec. Phys.*, **54**, 1261.
[23] STILLINGER, F. H., and RAHMAN, A., 1974, *Molecular Motions in Liquids*, edited by J. Lascombe (Reidel), p. 479.
[24] HERZBERG, G., 1960, *Molecular Spectra and Molecular Structure*, Vol. II (Van Nostrand).
[25] ROTHSCHILD, W. G., 1970, *J. chem. Phys.*, **53**, 3265.
[26] O'REILLY, D. E., PETERSON, E. M., and YASAITIS, E. L., 1972, *J. chem. Phys.*, **57**, 890.